

Magneto-electronic, and optical properties of reduced layered hybrid $\text{Zn}(\text{C}_4\text{H}_4\text{N}_2)\text{V}_4\text{O}_{10}$ complex: A DFT study

JUNAID MUNIR¹, AHMED S. JBARA², QURATUL AIN³, LAWAL MOHAMMED⁴, MASOOD YOUSAF^{5,*}

¹Department of Physics, Riphah International University, Lahore, Pakistan

²Physics Department, Science College, Al-Muthanna University, Samawah, 66001, Iraq

³Department of Physics, University Management Technology, Lahore, Pakistan

⁴School of Materials Science and Engineering, Yancheng Institute of Technology, Yancheng 224051, PR China

⁵Department of Physics, University of Education, Lahore, Pakistan

Optoelectronic response and half-magnetic behavior of layered organic-inorganic $\text{Zn}(\text{C}_4\text{H}_4\text{N}_2)\text{V}_4\text{O}_{10}$ hybrid complex have been investigated using full-potential linearized augmented plane wave (FP-LAPW) method with spin-polarized density functional theory. The density of states (DOS) reveals the exchange splitting of doubly degenerate (e_g) and triply degenerate (t_{2g}) states. The t_{2g} state is crossing the Fermi level which leads to 100% spin polarization of conduction electrons and confirms half-metallic nature near the Fermi level at equilibrium state with mBJ potential. Spin magnetic moments are associated with 3d orbitals of vanadium and zinc atoms which is the main contribution source to the overall magnetic moment of the complex. The band-gap accuracy is achieved with modified Becke-Johnson (mBJ) exchange potential. A band-gap of 3.81 eV is observed in the majority spin states with mBJ potential. In addition, the imaginary and real contributions of the dielectric function are also calculated. A maximum optical conductivity is achieved with mBJ potential. The present results confirm the half-metallic nature of the complex. The findings of the study endorse $\text{Zn}(\text{C}_4\text{H}_4\text{N}_2)\text{V}_4\text{O}_{10}$ complex as a potential applicant for next-generation spintronic and optoelectronic devices.

(Received October 5, 2020; accepted December 6, 2022)

Keywords: Half-metallic materials, First-principles calculations, Spin magnetic moment, Electronic structure, Spintronics

1. Introduction

Recently, a new design of coordination polymers based on the hybrid organic-inorganic composition has obtained much attention especially in the field of magnetism, conductivity, catalysis and optical behavior [1-6]. The appealing surface topologies of these polymers also make them a potential candidate regarding the applications in selective absorption, sensors, and luminescence [7-12]. Hybrid organic-inorganic bioceramics have a major role in cancer cell targeting nano-systems and stimuli-responsive systems of drug delivery [13-15]. Highly luminescent and ultra-stable $\text{CH}_3\text{NH}_3\text{PbBr}_3$ perovskites polymer films of composite possess unsurpassed heat and water stability [16]. Bis(trifluoromethanesulfonyl) amide (LiTFSI) is considered as a suitable candidate for the applications of solid-state lithium batteries [17]. Electrolyte membranes based on nano-composite polymers are also used in fuel cells [18]. Recently, organic-inorganic composites have gained much attention of the researchers for multiple applications [19-27]

Layered vanadates have gained much attention as quantum spin ($S=1/2$) low dimensional systems with a notable example of extended spin systems, ladders and spin dimers having charge-ordered or spin gap states [28, 29]. These coordination complexes become more inimitable with the presence of bridging ligands like pyridine, pyrazine or bi-pyridine. The magnetic behavior of these complexes containing Co, Cu, Mn or Ni and pyrazine are studied either with theory or experiment [30-35]. In ferroelectric organic-

inorganic hybrid compounds, spontaneous switchable polarization provides a strong photoluminescence emission which shows high luminescence with a benefit of ferroelectricity [36]. Methylammonium Bismuth Iodide is a potential candidate as a solar absorber because of its lead-free stability [37]. The bridging ligand is very important in mediating delocalization between charge centers and electronic communication in near delocalized mixed valence complexes [38]. Recently, organic-inorganic hybrid of perovskite, $(\text{C}_{12}\text{H}_{22}\text{N}_2)[\text{CuCl}_4]$, bis tetrachloridomanganate and many more have attracted the attention of the researchers [39-42]. The present work explores the structural, optical, magnetic and electronic properties of layered pyrazine based vanadate hybrid complex.

$\text{Zn}(\text{C}_4\text{H}_4\text{N}_2)\text{V}_4\text{O}_{10}$ ($\text{C}_4\text{H}_4\text{N}_2$ =pyrazine) is an important layered vanadate of hybrid organic-inorganic family. It has an orthorhombic structure with space group 63Cmcm . So far, no detailed work based on the density functional theory is conducted to explore the potential of the complex for practical application. This work includes an extensive study of structural, magnetic, optical and electronic properties with local spin density approximation (LSDA), generalized gradient approximation (GGA) along with modified Becke-Johnson (mBJ) exchange potential approximations.

The crystallographic data of this compound is taken from [35]. It contains 50 atoms in the orthorhombic primitive unit cell with $2/m$ symmetry. It also contains layers of $\text{V}_4\text{O}_{10}^{2-}$ which are charge-balanced and bounded by the layers of $\text{M}(\text{pyz})^{+2}$. The hydrogen (H) atoms are at

ideal positions in the structure which allow them to move on the parent carbon atoms. The lattice constants for Zn(C₄H₄N₂)V₄O₁₀ are: $a=14.4247\text{\AA}$, $b=6.9701\text{\AA}$ and $c=11.4792\text{\AA}$.

2. Computational details

For calculation purposes, density functional theory is employed via wien2k code which is based on the linearized augmented plane wave (LAPW) and full-potential-LAPW methods and considered as an accurate method to calculate electronic properties [43]. For structural properties, generalized gradient approximation is treated with exchange-correlation interactions as Perdew-Burke Ernzerhof 96 (PBE-GGA) parameterized it [44, 45].

The band-gap accuracy is achieved with modified Becke-Johnson (mBJ) exchange potential with LDA or GGA correlation through spin polarization. mBJ introduced the 'c' parameter in the original exchange mBJ potential [46].

$$v_{\chi,\sigma}^{mBJ}(r) = cv_{\chi,\sigma}^{BR}(r) + (3c - 2) \frac{1}{\pi} \sqrt{\frac{5}{12}} \sqrt{\frac{2t_{\sigma}(r)}{n_{\sigma}(r)}} \quad (1)$$

where t_{σ} represents kinetic energy density and n_{σ} is the electron density and both spin-dependent while $v_{\chi,\sigma}^{BR}$ is Becke-Roussel potential [47]. The parameter 'c' can be determined as:

$$c = \alpha + \beta \left(\frac{1}{V_{cell}} \int_{cell} \frac{|\nabla n(r')|}{n(r')} d^3r' \right)^{1/2} \quad (2)$$

where cell volume is V_{cell} . The parameters α and β are selected in the widespread scope of solids to fit a band-gap. GGA correlation and exchange both potentials are used in mBJ approximation which results in accurate band-gap calculations [46]. The muffin tin radii (a.u) selected for atoms of Zn =2.07, V = 1.63, O =1.44, N=1.20, C=1.17 and H=0.63. With respect to crystal harmonics, the charge and

potential density inside the atomic spheres are extended up to angular momentum with a value of 10. The density plane wave cut-off (RK_{max}) value is set to 3 because of the hydrogen presence. The cell has been divided during the calculations into two regions; one is an interstitial region which does not included in the atomic spheres and the other is non-overlapping atomic spheres region. The interstitial region doesn't include in atomic spheres. The maximum reciprocal vector for fourier expansion of electron density is $G_{max} = 20$. The self-consistency with a value of 0.0001Ry is achieved.

3. Results and discussions

The electronic band structure of the complex Zn(C₄H₄N₂)V₄O₁₀ for both spin up and down with greater symmetry lines across the 1st Brillouin zone is computed with LDA, PBE-GGA, and mBJ-PBE-GGA approximations. Figs. 1, 2 and 3 show a band-gap which confirms a semiconductor behavior at the Fermi level of this complex in majority spin-gap, however the minority spin-gap shows a conducting behavior with LDA, PBE-GGA and mBJ potentials respectively. A band-gap of 2.28eV, 2.79eV and 3.81eV in spin-up states is obtained with LDA, GGA and mBJ potentials, respectively. In the case of spin-down states, a band-gap of 0.47eV and 0.54 eV is achieved with LDA and GGA potentials while a metallic nature is observed with mBJ potential. The total energy calculations can be misinterpreted with the use of LDA and GGA potentials. For electronic calculations, LDA underestimates the electronic band-gap of materials as pointed out by Perdew et al. [48]. This underestimation in band-gap for semiconductors and insulators is approximately 40% of the real value. To negate this issue, an exchanged potential named modified Becke-Johnson (mBJ) is utilized, which improve the band-gap values [46]. Thus, half-metallic ferro-magnets can be described more suitably with mBJ rather than with LDA and GGA both. Fig. 1. Electronic spin-polarized band structure (for both spin-states) of Zn(C₄H₄N₂)V₄O₁₀ with PBE-GGA.

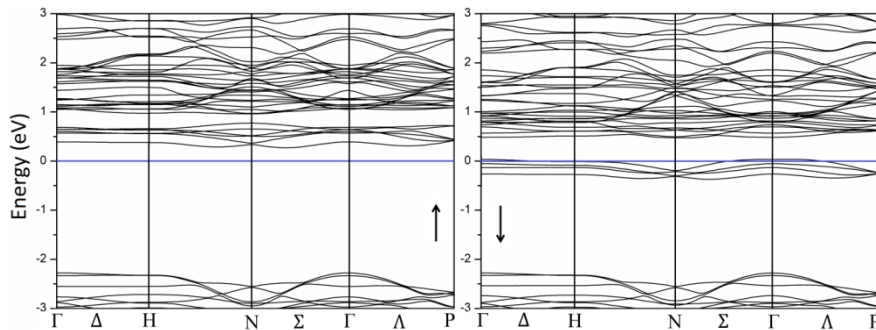


Fig. 1. Electronic spin-polarized band structure (for both spin-states) of Zn(C₄H₄N₂)V₄O₁₀ with LDA (color online)

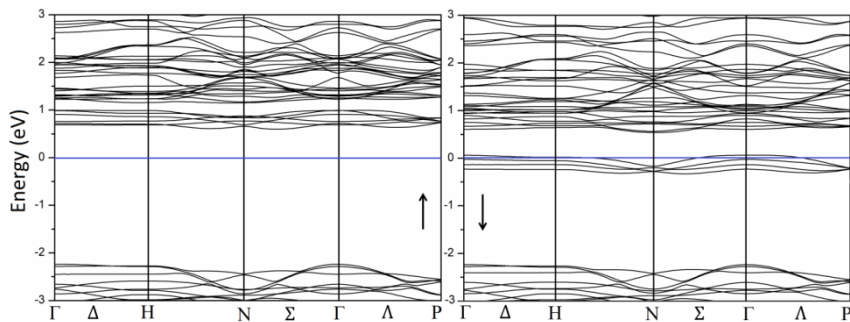


Fig. 2. Electronic spin-polarized band structure (for both spin-states) of $\text{Zn}(\text{C}_4\text{H}_4\text{N}_2)\text{V}_4\text{O}_{10}$ with PBE-GGA

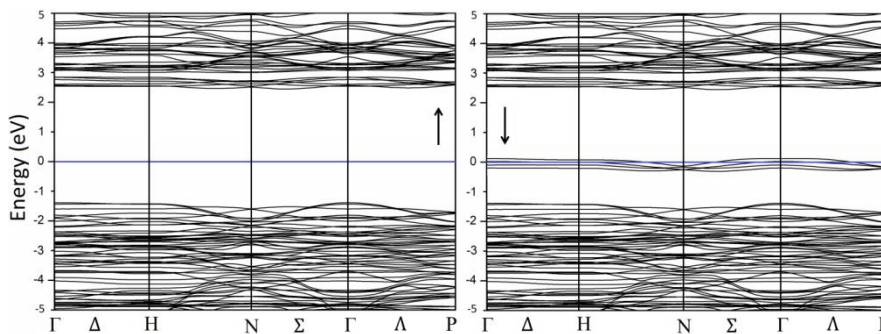


Fig. 3. Electronic spin-polarized band structure (for both spin-states) of $\text{Zn}(\text{C}_4\text{H}_4\text{N}_2)\text{V}_4\text{O}_{10}$ with mBJ-PBE-GGA

The distribution of the total and partial density of states (DOS) is used to determine the magnetic properties near the Fermi level. In the present case, the ordered spin arrangement is caused by the exchange interaction which results in the clear splitting of total DOS. The total number of unpaired electrons is responsible for the magnetic moments. It is also observed from DOS distribution that the 3d-V orbital is the key source of magnetism because of the available unpaired electrons. The spin-polarized partial and total DOS are presented with LDA (Fig.4), PBE-GGA (Fig. 5) and PBE-mBJ (Fig. 6). The exchange interaction is caused by 3d orbital in transition elements because of its unpaired spins shape and prevalence. The d orbital splits into low energy, doubly degenerate (e_g) consists of $d_z^2, d_{x^2-y^2}$ states and triply degenerate (t_{2g}) consist of d_{xy}, d_{yz}, d_{xz} states can be explained with crystal field theory and represented in Figs. 4, 5 and 6.

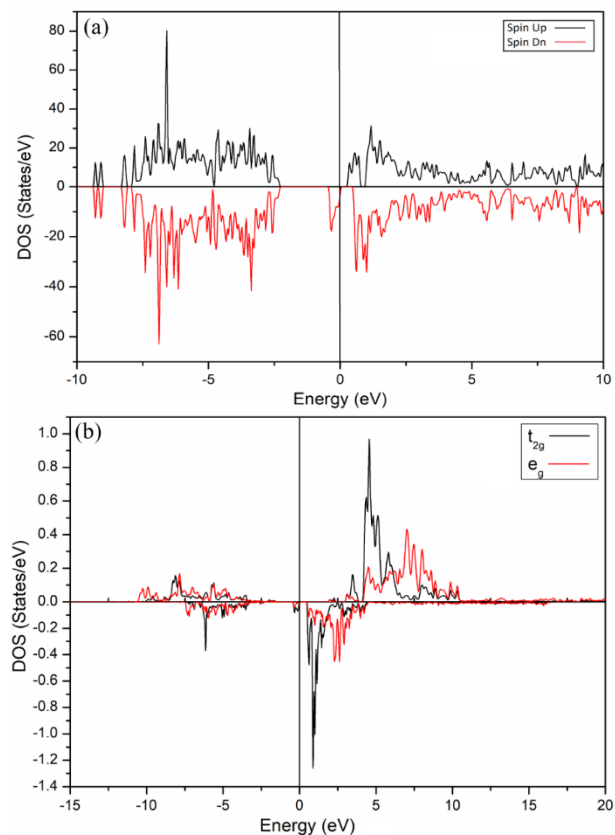


Fig. 4. Total (a) and partial (b) spin-polarized DOS of $\text{Zn}(\text{C}_4\text{H}_4\text{N}_2)\text{V}_4\text{O}_{10}$ with LDA (color online)

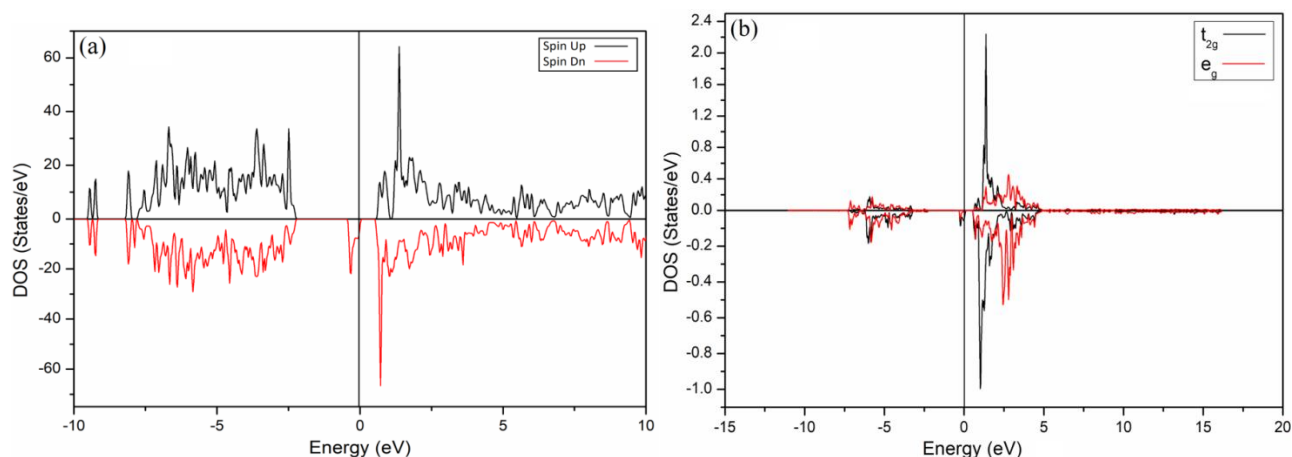


Fig. 5. Total (a) and partial (b) spin-polarized DOS of $\text{Zn}(\text{C}_4\text{H}_4\text{N}_2)\text{V}_4\text{O}_{10}$ with PBE-GGA (color online)

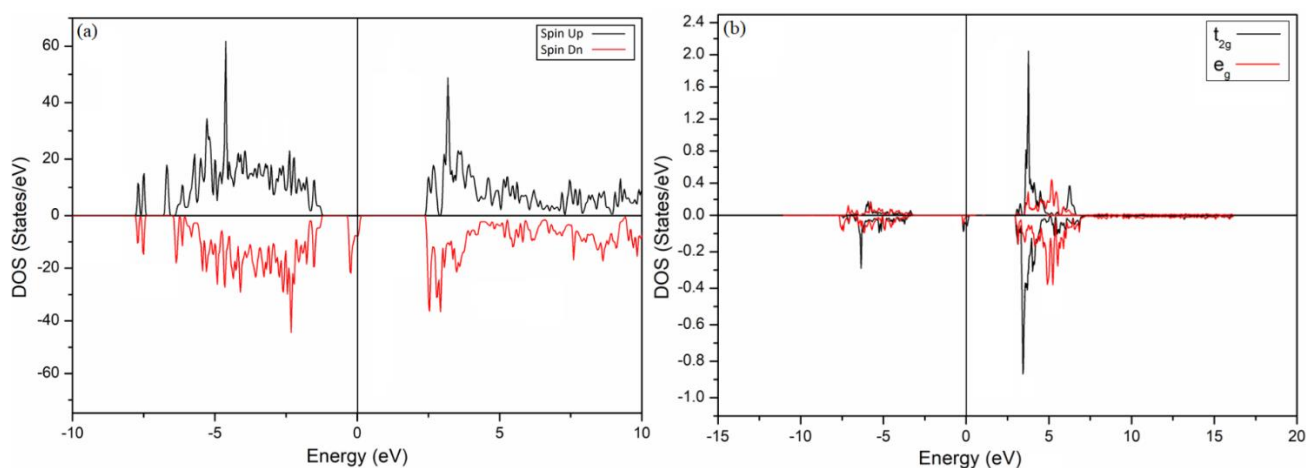


Fig. 6. Total (a) and partial (b) spin-polarized DOS of $\text{Zn}(\text{C}_4\text{H}_4\text{N}_2)\text{V}_4\text{O}_{10}$ with mBJ-PBE-GGA (color online)

The interaction among ligands and transition metal occurs from the interaction between the $-ve$ charge on the nonbonding ligand's electrons and $+ve$ charged metal cation which causes to yield crystal field splitting. It is most probably due to the interaction among the lobes of d-orbital and the ligand field. There is a wider spin-up band-gap in PBE-mBJ case than LDA and PBE-GGA. There is also observed a metallic nature by applying LDA, PBE-GGA and PBE-mBJ potentials at equilibrium state which confirms a half-metallic electronic character of this complex using these approximations. At the Fermi level, the conducting electrons are fully spin-polarized because the t_{2g} and e_g states crossing the Fermi level.

Orthorhombic structure (simulated) for unit cell of complex $\text{Zn}(\text{C}_4\text{H}_4\text{N}_2)\text{V}_4\text{O}_{10}$ is shown in Fig. 7.

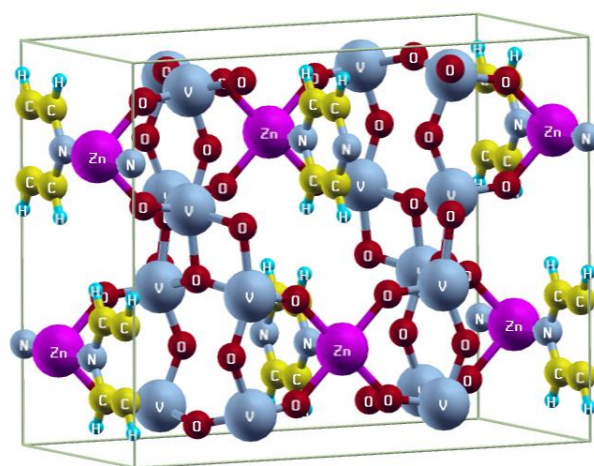


Fig. 7. Unit cell orthorhombic structure of $\text{Zn}(\text{C}_4\text{H}_4\text{N}_2)\text{V}_4\text{O}_{10}$ complex (color online)

It can be seen from the analysis of electronic structure (Table 1) that the 3d-states of vanadium and zinc atoms are mainly responsible for spin-population; however, the other orbitals have negligible contribution. Table 1 shows the spin magnetic moment inside the atomic sphere. The

magnetic ions of a molecule are responsible for the total magnetic moment. The calculated results exhibit that the spin populations on hydrogen atoms are very small and can be neglected. Therefore, spin populations of vanadium, zinc, nitrogen, oxygen, and carbon are presented in the table. $Zn(C_4H_4N_2)V_4O_{10}$ is a bi-nuclear compound because of two magnetic centers of Zn and V ions. These spin populations show strong positivity for vanadium and zinc cations,

slightly positive for nitrogen and negative on one oxygen and carbon anions. The spin polarization effect is the source of V-Zn and V-V interactions and spin delocalization effect cause the Ni-Ni interaction.

Table 1. Spin magnetic moment inside the atomic sphere of various atomic sites

Atomic Position	Spin-Population	Atomic Position	Spin-Population
Zn (3-d)	1.0175	O1 (2-p)	-0.0013
V (3-d)	1.4370	O2 (2-p)	0.0210
N1 (2-p)	0.0017	O3 (2-P)	0.0686
N2 (2-p)	0.0020	C1 (2-p)	-0.0006

The electron density plots corresponding to the crystallographic plane of $Zn(C_4H_4N_2)V_4O_{10}$ displaying the bonding character along [100] plane and [110] plane are shown in Fig. 8. It is observed from these plots that there no

major change in both spin-up and down cases for [100] and [110] planes. A small variation in the color scale is observed, which can be caused by the non-metallic behavior in spin-up and metallic nature in spin-dn states, respectively.

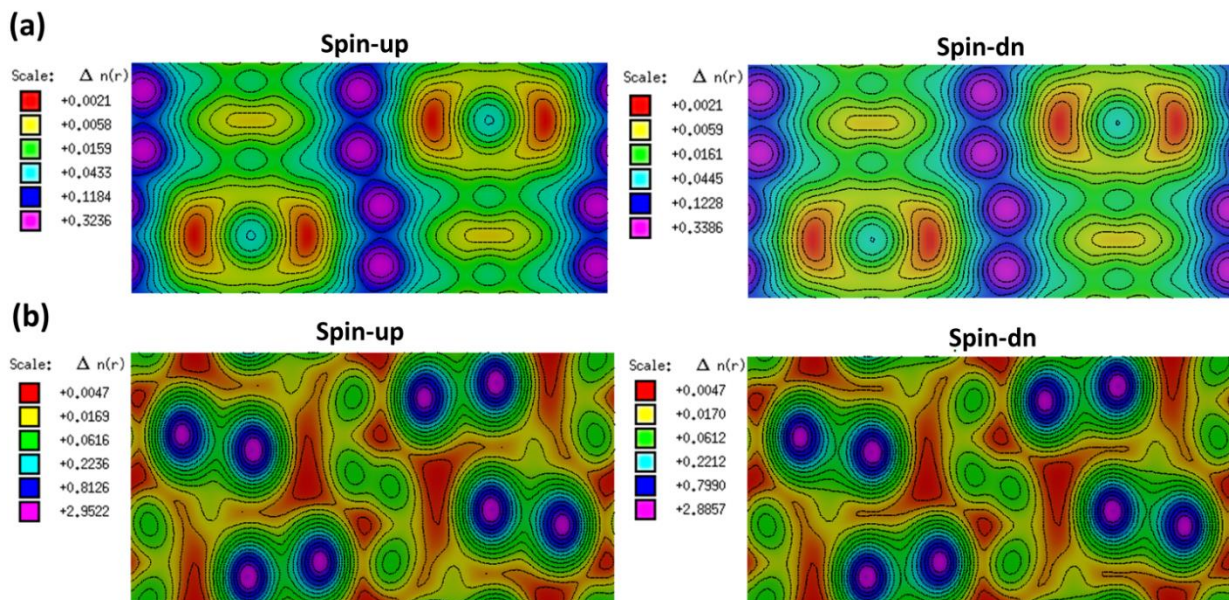


Fig. 8. Contour plots along (a) [100], and (b) [110] planes of electron charge density (color online)

The bonding nature between anions and cations is described with these electron charge density plots. The charge density distribution among cations and anions shows a more spherical nature in [110] plane which predicts the ionic nature while in [100] plane a charge distribution is observed which indicate the covalent nature. Strong covalent bonding is indicated through C-H bond and the covalent nature is dominated because of strong hybridization. The electronegativity among atoms causes the electron density plot. A few small vacancies can also be observed which are created by the absence of charge density and ions can occupy their places. In conclusion, a mixed nature i.e., both ionic and covalent bonding is observed in the complex.

Optical properties are very important in providing useful information about the internal structure of

compounds. When the light incident on the compound surface is partially transmitted and partially reflected. The reflected light includes the information about the physical properties such as their vibrational and electronic states and also the nature and existence of impurities and defects in the crystal structure. The following relations are used to figure out the imaginary and real both contributions of dielectric function [49].

$$\varepsilon_1(\omega) = 1 + \frac{2}{\pi} P \int_0^{\infty} \frac{\omega' \varepsilon_2(\omega')}{\omega'^2 - \omega^2} d\omega' \quad (3)$$

$$\varepsilon_2(\omega) = \frac{8}{2\pi\omega^2} \sum_{nn'} |P_{nn'}|^2 \frac{dS_k}{\nabla\omega_{nn'}(k)} \quad (4)$$

where the dipole matrix element is represented with $P_{nn'}$, the energy difference is given with $\omega_{nn'}(k)$, surface energy

with constant value is S_k and Cauchy principal values is represented with P. The imaginary segment for the dielectric function is presented in Fig. 9 and the real part is presented in Fig. 10.

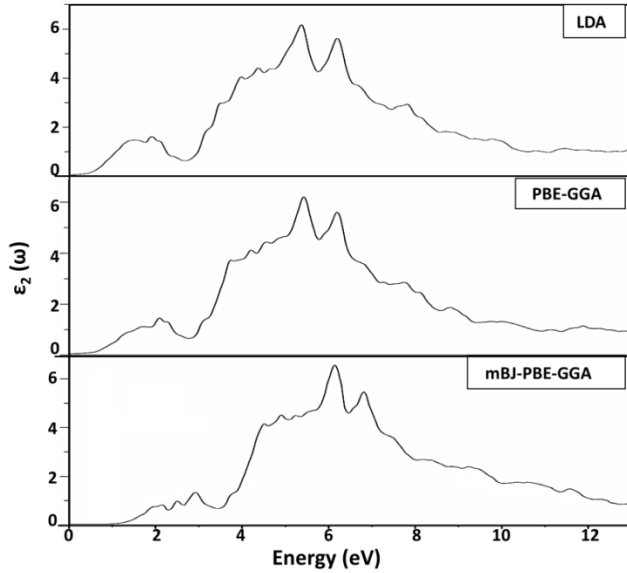


Fig. 9. Dielectric function's imaginary part for orthorhombic structure of $\text{Zn}(\text{C}_4\text{H}_4\text{N}_2)\text{V}_4\text{O}_{10}$

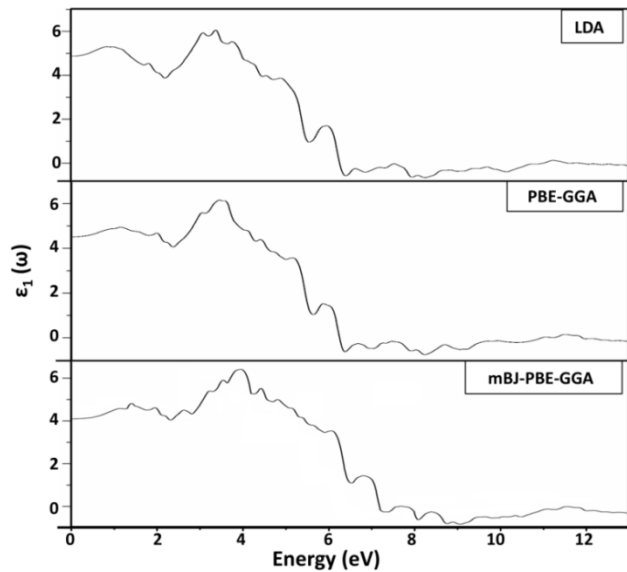


Fig. 10. Dielectric function's real part for orthorhombic structure of $\text{Zn}(\text{C}_4\text{H}_4\text{N}_2)\text{V}_4\text{O}_{10}$

Dielectric function is used to investigate the material's optical properties. In optical axes of the imaginary part, the offset points show the optical gap and these points are observed at different points for all potentials. The real part which is a very significant factor of the dielectric function shows its peaks at 3.4, 3.6 and 3.9 for LDA, PBE-GGA, and mBJ-PBE-GGA respectively. In the imaginary part, the optical spectra are shifted towards the region of high energy, as shifting from LDA towards mBJ-PBE-GGA. The reason for this shifting is the increase in band-gap values. The increase in the band-gap value causes to increase in

threshold energy of the major excitation in imaginary part. As a result, spectra in imaginary part experiencing a blue shift and it is comparable to the other research work [50, 51]. All graphs shift from low to high energies with mBJ potential and with lower amplitude, it produces a better band splitting as presented in [52].

The electron's conductivity in the photon field is provided with optical conductivity. The real component of optical conductivity for $\text{Zn}(\text{C}_4\text{H}_4\text{N}_2)\text{V}_4\text{O}_{10}$ with LDA, PBE-GGA and mBJ-PBE-GGA is presented in Fig. 11. It can be seen from these all three potentials that there is no conduction at critical point i.e. zero energy which confirms the existence of the optical band-gap. The critical points are at 0.58eV for LDA, 0.63eV for PBE-GGA and 1.3eV for mBJ-PBE-GGA. There is an increase in conductivity and it attained its maximum value at particular energy beyond the critical points. It can be easily observed that the conductivity is larger for mBJ potential as compared to LDA and GGA.

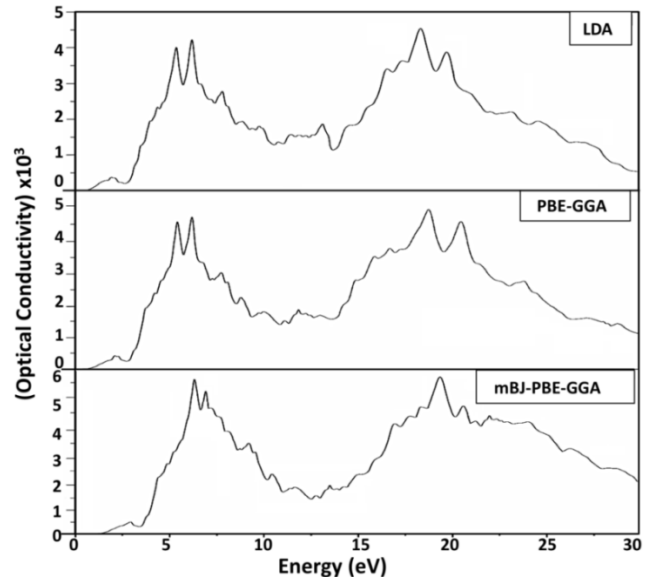


Fig. 11. The optical conductivity vs energy plot for real part of $\text{Zn}(\text{C}_4\text{H}_4\text{N}_2)\text{V}_4\text{O}_{10}$

The increase in band-gap causes to increase in optical conductivity. More energy is required by electrons to cross the Fermi level which results in the maximum value of optical conductivity.

4. Conclusion

The hybrid layered $\text{Zn}(\text{C}_4\text{H}_4\text{N}_2)\text{V}_4\text{O}_{10}$ complex in the orthorhombic phase has been investigated theoretically. A band-gap in both majority and minority states is observed with LDA and GGA potentials. The majority and minority spin states reveal a large exchange splitting. In the case of mBJ, a band gap is observed in majority spin states and minority spin shows the crossing of t_{2g} state at Fermi level. Zinc and Vanadium cations have shown significant spin magnetic moments which points out the ferromagnetic interactions and it confirms the availability of this complex

as a relevant candidate for future spintronic devices. The electronic properties suggest the availability of the studied compound for spintronic devices. The maximum optical conductivity is achieved with mBJ potential. An optical gap of 1.8eV is also observed with the mBJ potential, endorsing its suitability for the optoelectronic applications.

References

- [1] W. Kobel, M. Hanack, *Inorganic Chemistry* **25**(1), 103 (1986).
- [2] C.-T. Chen, K. S. Suslick, *Coordination chemistry reviews* **128**(1-2), 293 (1993).
- [3] C. Janiak, *Angewandte Chemie International Edition in English* **36**(13-14), 1431 (1997).
- [4] Yuichi Sugiyama, Keiichi Adachi, Satoshi Kawata, Hitoshi Kumagai, Katsuya Inoue, Motomi Katada, Susumu Kitagawa, *Cryst. Eng. Comm.* **2**(32), 174 (2000).
- [5] Jonas A. Schwenzler, Tim Hellmann, Bahram Abdollahi Nejand, Hang Hu, Tobias Abzieher, Fabian Schackmar, Ihteaz M. Hossain, Paul Fassel, Thomas Mayer, Wolfram Jaegermann, Uli Lemmer, Ulrich W. Paetzold, *ACS applied materials & interfaces* **13**(13), 15292 (2021).
- [6] Wail Al Zoubi, Muhammad Prisla Kamil, Siti Fatimah, Nisa Nashrah, Young Gun Ko, *Progress in Materials Science* **112**, 100663 (2020).
- [7] A. U. Czaja, N. Trukhan, U. Müller, *Chemical Society Reviews* **38**(5), 1284 (2009).
- [8] M. D. Allendorf, C. A. Bauer, R. K. Bhakta, R. J. T. Houk, *Chemical Society Reviews* **38**(5), 1330 (2009).
- [9] Qing Chen, Jian-Bin Lin, Wei Xue, Ming-Hua Zeng, Xiao-Ming Chen, *Inorganic Chemistry* **50**(6), 2321 (2011).
- [10] Francesco Radica, Stefania Mura, Davide Carboni, Luca Malfatti, Sebastiano Garroni, Stefano Enzo, Giancarlo Della Ventura, Giovanna Tranfo, Augusto Marcelli, Plinio Innocenzi, *Microporous and Mesoporous Materials* **294**, 109877 (2020).
- [11] Zhihui Ren, Juehan Yang, Dongchen Qi, Prashant Sonar, Liyuan Liu, Zheng Lou, Guozhen Shen, Zhongming Wei, *Advanced Materials Technologies* **6**(4), 2000889 (2021).
- [12] P. Pacchin Tomanin, *Engineering catalytic organic-inorganic materials for sensing applications*, 2020.
- [13] M. Vallet-Regí, M. Colilla, B. González, *Chemical Society Reviews* **40**(2), 596 (2011).
- [14] Danushika C. Manatunga, V. Umayangana Godakanda, Rohini M. de Silva, K. M. Nalin de Silva, *Wiley Interdisciplinary Reviews: Nanomedicine and Nanobiotechnology* **12**(3), e1605 (2020).
- [15] F. Bollino, M. Catauro, *Macromolecular Symposia*. 2020, Wiley Online Library.
- [16] Yanan Wang, Juan He, Hao Chen, Jiangshan Chen, Ruidong Zhu, Pin Ma, Andrew Towers, Yuan Lin, Andre J. Gesquiere, Shin-Tson Wu, Yajie Dong, *Advanced Materials* **28**(48), 10710 (2016).
- [17] Dong-Gyun Kim, Jimin Shim, Jin Hong Lee, Su-Jee Kwon, Ji-Hoon Baik, Jong-Chan Lee, *Polymer* **54**(21), 5812 (2013).
- [18] Mashallah Rezakazemi, Mohtada Sadrzadeh, Toraj Mohammadi, Takeshi Matsuura, *Organic-inorganic composite polymer electrolyte membranes*, Springer, 311 (2017).
- [19] Dianlong Zhao, GuanJun Xiao, Zhun Liu, Laizhi Sui, Kaijun Yuan, Zhiwei Ma, Bo Zou, *Advanced Materials* **33**(31), 2100323 (2021).
- [20] M. Razizadeh, M. Mahdavian, B. Ramezanzadeh, E. Alibakhshi, S. Jamali, *Construction and Building Materials* **287**, 123034 (2021).
- [21] Jie Yao, Qiang Pan, Zi-Jie Feng, Yu-An Xiong, Tai-Ting Sha, Hao-Ran Ji, Zhu-Xiao Gao, Yu-Meng You, *APL Materials* **9**(4), 040901 (2021).
- [22] Hadiyah Fattal, Tielyr D. Creason, Cordell J. Delzer, Aymen Yangui, Jason P. Hayward, Bradley J. Ross, Mao-Hua Du, Daniel T. Glatzhofer, *Inorganic Chemistry* **60**(2), 1045 (2021).
- [23] C. A. Aranda, L. Calì, M. Salado, *Crystals* **11**(5), 519 (2021).
- [24] C. Mendes-Felipe Antonio Veloso-Fernández, José Luis Vilas-Vilela, Leire Ruiz-Rubio, *Catalysts* **12**(2), 180 (2022).
- [25] W.-J. Xu, Svitlana Kopyl, Andrei Kholkin, João Rocha, *Coordination Chemistry Reviews* **387**, 398 (2019).
- [26] W.-J. Wei Chao Li, Lin-Sui Li, Yun-Zhi Tang, Xing-Xing Jiang, Zhe-Shuai Lin, *Journal of Materials Chemistry C* **7**(38), 11964 (2019).
- [27] Jingying Wang, Chuang Zhang, Haoliang Liu, Xiaojie Liu, Hangwen Guo, Dali Sun, Zeev Vally Vardeny, *Advanced Materials* **31**(41), 1904059 (2019).
- [28] Y. Ueda, *Chemistry of Materials* **10**(10), 2653 (1998).
- [29] T. Chirayil, P. Y. Zavalij, M. S. Whittingham, *Chemistry of materials* **10**(10), 2629 (1998).
- [30] Anamika Das, Iliya Todorov, Subrata K. Dey, Samiran Mitra, *Inorganica Chimica Acta* **359**(7), 2041 (2006).
- [31] H. Kumagai, S. Kawata, S. Kitagawa, *Inorganica Chimica Acta* **337**, 387 (2002).
- [32] K. Travis Holman, Hassan H. Hammud, Samih Isber, Malek Tabbal, *Polyhedron* **24**(2) 221 (2005).
- [33] Jamie L. Manson, Marianne M. Conner, John A. Schlueter, Kylee A. Hyzer, *Polyhedron* **26**(9-11), 1912 (2007).
- [34] P. Jensen Stuart R. Batten, Boujemaa Moubaraki Keith S. Murray, *Journal of Solid State Chemistry* **159**(2), 352 (2001).
- [35] Bangbo Yan, Junhua Luo, Paul Dube, Athena S. Sefat, John E. Greedan, Paul A. Maggard, *Inorganic Chemistry* **45**(13), 5109 (2006).
- [36] Heng-Yun Ye, Qiong Hua Zhou, Xiang Hong Niu, Wei-Qiang Liao, Da-Wei Fu, Yi Zhang, Yu-Meng You, Jinlan Wang, Zhong-Ning Chen,

- Ren-Gen Xiong, *Journal of the American Chemical Society* **137**(40), 13148 (2015).
- [37] R. L. Hoye, *Chemistry-A European Journal* **22**(8), 2605 (2016).
- [38] C. H. Londergan, C. P. Kubiak, *The Journal of Physical Chemistry A* **107**(44), 9301 (2003).
- [39] M. Fizer Mikhailo Slivka, Vasyl Sidey, Vyacheslav Baumer, Ruslan Mariychuk, *Journal of Molecular Structure* **1235**, 130227 (2021).
- [40] H. Ferial Youssef Arfaoui, Cristian Silvestru, Noura Fakhar Bourguiba, *Journal of Coordination Chemistry*, 1 (2022).
- [41] A. Khadri, Rafika Bouchene, Sofiane Bouacida, Assia Sid, Ibrahim A. Alswaidan, Ponnadurai Ramasami, *Journal of Coordination Chemistry* **73**(4), 609 (2020).
- [42] Y. J. Cao, Lin Zhou, Lei He, Ping-Ping Shi, Qiong Ye, Da-Wei Fu, *Chemistry-A European Journal* **26**(62), 14124 (2020).
- [43] P. Blaha, Karlheinz Schwarz, Georg K. H. Madsen, Dieter Kvasnicka Joachim Luitz, Robert Laskowski, Fabien Tran, Laurence D. Marks, An augmented plane wave+ local orbitals program for calculating crystal properties, 2001.
- [44] J. P. Perdew, K. Burke, Y. Wang, *Physical Review B* **54**(23), 16533 (1996).
- [45] J. P. Perdew, K. Burke, M. Ernzerhof, *Physical Review Letters* **77**(18), 3865 (1996).
- [46] F. Tran, P. Blaha, *Physical review letters* **102**(22), 226401 (2009).
- [47] A. Becke, M. R. Roussel, *Physical Review A* **39**(8), 3761 (1989).
- [48] J. P. Perdew, M. Levy, *Physical Review Letters* **51**(20), 1884 (1983).
- [49] M. Fox, *Optical properties of solids*, American Association of Physics Teachers, 2002.
- [50] A. K. Sharma, J. Thakur, M. K. Kashyap, *AIP Conference Proceedings*, American Institute of Physics, 2014.
- [51] S. Shabbir, A. Shaaria Bakhtiar Ul Haq, R. Ahmed, S. AlFaify, M. Ahmed. A. Laref, *Materials Science in Semiconductor Processing* **121**, 105326 (2021).
- [52] A. Reshak, H. Kamarudin, S. Auluck, *The Journal of Physical Chemistry B* **116**(15), 4677 (2012).

*Corresponding author: masood.yousaf@ue.edu.pk